Trapping and detecting trace radioactive isotopes produced in ICF implosions

Mark Yuly, Stephen Padalino, Adam Brown, Andrew Hotchkiss, Chunsun Lei, Andrew Martin.

I. Measuring Nuclear Cross Sections Low-Energy Light Ion Reactions using ICF

This report describes continuing work to develop a system for measuring cross sections for low-energy light ion nuclear reactions with applications in astrophysics, especially stellar and big bang nucleosynthesis, and thermonuclear fusion diagnostics. Because most cross sections at these low keV energies have never been measured, primordial nucleosynthesis models, for example, often resort to cross sections extrapolated downward in energy by many orders of magnitude. Occasionally, when higher energy measurements are not available for extrapolation, some reactions are even left out of the nucleosynthesis models [1]. All of this leads to uncertainty in the model isotope abundance predictions; for example, some overpredict the abundance of ^{7}Li while simultaneously underpredicting ^{6}Li [2, 3]. Additionally, as a thermonuclear fusion diagnostic, light ion radiative capture reactions have been suggested [4, 5, 6] for high temperature DT plasmas and have been observed experimentally in plasmas at thermonuclear temperatures [7, 8, 9, 10].

These low-energy cross sections have never been measured because of the difficulty presented in using traditional accelerator experiments. The same number of nuclear reactions that would take months or even years to produce with a traditional accelerator experiment could be produced in a nanosecond using inertial confinement fusion (ICF), and, moreover, the measurement would take place in a more relevant plasma environment.

Table 1 shows some of the highest yield reactions that might be measurable with ICF using the OMEGA-60 laser at the Laboratory for Laser Energetics (LLE). These triton reactions typically have no threshold energy, and would yield 10^5 to 10^6 product nuclei per shot, of either ^{6}He or ^{8}Li, both of which decay by beta emission, with similar half-lives of 807 ms and 840 ms respectively. The beta endpoint energy for ^{8}Li is not a constant value because the transition is to a broad excited state of ^{8}Be at 3.03 MeV, but the beta spectrum has its peak at around 6 MeV and extends to energies above 13 MeV! The endpoint energy for ^{6}He is 3507.8 MeV and the average is 1567.6 MeV.

Table 1. Estimated yields for the most prolific light ion reactions that may be studied using our technique. The prediction assumes the target capsule is doped with 1% of the appropriate reactant isotope. Shot parameters for OMEGA shot 77951 were used, a tritium-filled SiO_2 capsule "exploding pusher" that reached 18.3 keV. For ^{3}H(t,γ)^{6}He the predicted yield is based on assuming a branching ratio of 10^{-7}, which is simply an estimated "best case". For other reactions, reactivities were estimated using S-factor extrapolations [11] and TALYS-1.9 [12].

Reaction	Product Half-life	Reactant Abundance	Predicted Yield
^{3}H(t,γ)^{6}He	807 ms	10^{-7} branching	8×10^{4}
^{6}Li(t,p)^{8}Li	840 ms	7.6%	$0.2\text{-}1\times10^{7}$
^{7}Li(t,α)^{6}He	807 ms	92.4%	$0.7\text{-}2\times10^{6}$
^{9}Be(t,α)^{8}Li	840 ms	100%	5×10^{5}

In the ICF process, lasers strike and compress the target capsule, raising the temperature at the center high enough for DT fusion and other nuclear reactions to occur. By doping the target with the desired reactant (i.e. ^{3}H fill, ^{6}Li, ^{7}Li or ^{9}Be for the reactions in Table 1) it would be possible to cause these reactions to occur. Afterward, the expanding plasma containing the reaction products (e.g. ^{6}He or ^{8}Li) will cool and recombine to form a neutral gas. To measure the reactivity then, some of this gas could be collected, and the beta decays of the product nuclei counted.

This has the advantage that the detector will be operating milliseconds after the shot, in the relatively quiet environment after the gamma rays, neutrons and EMP have all passed. Moreover, since the decay rate will be relatively low, individual detector pulses could be counted, and particle identification could be performed event-by-event. This is typically not the case for most ICF experiments, which look at primary radiation. Although the background rate will be much lower after the shot, there nevertheless will be background due to activation of the surrounding material by primary neutrons. While detector particle identification will help, separating beta particles from gamma rays will still be a problem.

The basic idea of the experiment is shown in Figure 1 for two different traps: a turbopump (left), which would allow chemically non-reactive products like ^{6}He to be collected by trapping them in a hollow phoswich detector where they will decay, and a getter (right) for chemically reactive products like ^{8}Li, which hopefully will stick to and decay on the getter foil, and be detected by the phoswich scintillators. A phoswich detector, which has the advantage of being read out using a single phototube, consists of a fast, thin plastic scintillator (dE) followed by a slow, thick plastic scintillator (E). Since charged particles with different mass and charge deposit energy at different rates when slowing down in the scintillator, the pulse heights from the two scintillators can be used to identify the particle.

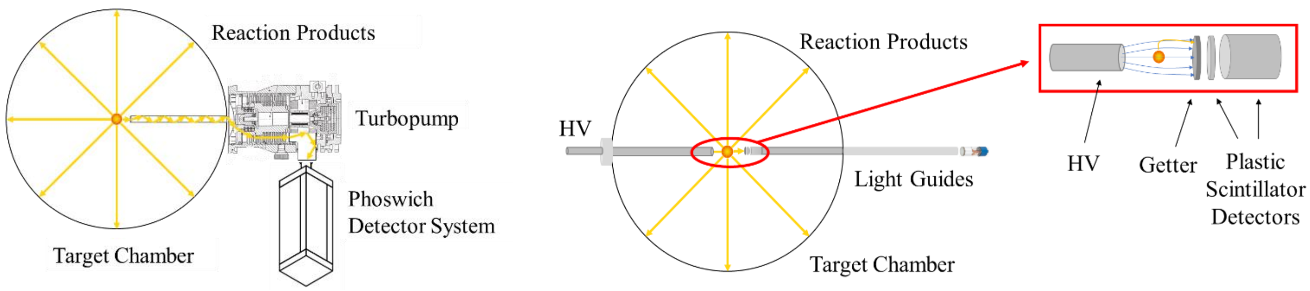

Figure 1. Techniques for capturing and detecting product nuclei. In the turbopump trap (left) the neutral gas containing the product nuclei enters a long tube that directs it into a turbopump. The turbopump output port leads the gas to a hollow rectangular 4π phoswich detector where the gas is trapped and product nuclei decays are counted. In the getter trap (right) the atoms containing product nuclei chemically bind to the getter material, and the decays are counted by a small phoswich detector behind the getter. It may be possible to use an electric field to ionize and cause inert atoms to implant into the getter.

The feasibility of an experiment similar to those shown in Figure 1 has been studied over the past six summers by faculty and students at Houghton College and SUNY Geneseo, and these experiments have been reported in three Houghton student theses [13, 14, 15], numerous posters presented at physics meetings, and in the annual progress reports from each summer. In 2016 [16] the initial conceptual work was carried out, and it was demonstrated that ^{6}He could be created and detected using a silicon dE-E detector telescope. The first simple phoswich detector, needed to withstand the ICF environment, was designed, built and tested on ^{6}He in 2017 [17]. In 2018 [18], more sophisticated calculations for estimated ICF yields were made for all of the most likely reaction candidates, and a vacuum system was constructed and tested for the purpose of studying traps and detectors by simulating the expanding radioactive gas produced by an ICF implosion. In 2019 [19] the turbopump trap and 4π phoswich detector were constructed and tested by releasing, capturing and trapping radioactive ^{41}Ar, an inert gas chemically similar to ^{6}He. Beta decays were identified and counted, and the resulting decay curve used to determine the number of ^{41}Ar that were trapped. The getter detector was constructed in 2020 [20], and a Geant4 [21] code was created to simulate the detectors. Also in that year, background rates in both detectors were measured using high-yield DT shots on OMEGA-60 as part of a ride-along experiment. Finally, last summer [22] an experiment simulating trapping and detecting radioactive product nuclei after an ICF shot was carried out using the SUNY Geneseo Pelletron accelerator.

II. ICF Simulation Experiments

During the summers of 2021 and 2022 a series of experiments were preformed using the SUNY Geneseo Pelletron accelerator in order to simulate the release of radioactive products after the laser shot. In these experiments, a tungsten foil was coated with a thin layer of copper (2021), Teflon (2021, 2022) or lithium (2022), inserted into the evacuated Houghton test chamber, and activated with a deuteron beam via the $^{65}Cu(d,p)^{66}Cu$, $^{19}F(d,p)^{20}F$, and $^{7}Li(d,p)^{8}Li$ reactions respectively. The thin film was then rapidly evaporated by quickly heating the tungsten foil with an electrical current, and an attempt was made to trap the out streaming neutral atoms and to detect the decays of their radioactive nuclei. The purpose of these experiments is threefold:

1. To demonstrate that it is possible to create and trap a hot outward flowing short lived radioactive neutral gas, and to detect and count the radioactive decays. For this purpose, $^{65}Cu(d,p)^{66}Cu$ was selected as the

initial test material because past experience shows copper easily sticks to most metals and has a relatively short (at least, compared to ^{41}Ar) half-life of 5.12 min . The ^{19}F(d,p)^{20}F reaction was selected for its even shorter half live of 11.07 seconds and because when Teflon is pyrolyzed many of the resulting compounds are relatively inert, and therefore more like ^{6}He. Finally, ^{7}Li(d,p)^{8}Li was selected as the most stringent test, since it is the actual nuclear product of interest in some of the reactions, and therefore has an appropriate half-life of 840 ms.

2. To measure the fraction product nuclei that were captured and detected. To do this, both the initial amount created by the deuteron beam and the number detected must be measured, and the absolute detector efficiency must be calculated using the GEANT monte carlo detector simulation that was developed in 2020.

3. To study the effect of different materials and geometries on this ratio. To do this, we intend to use the results of those experiments to guide the development of a simple model that can be applied to ICF outflow, using methods similar to those used for thin film deposition models.

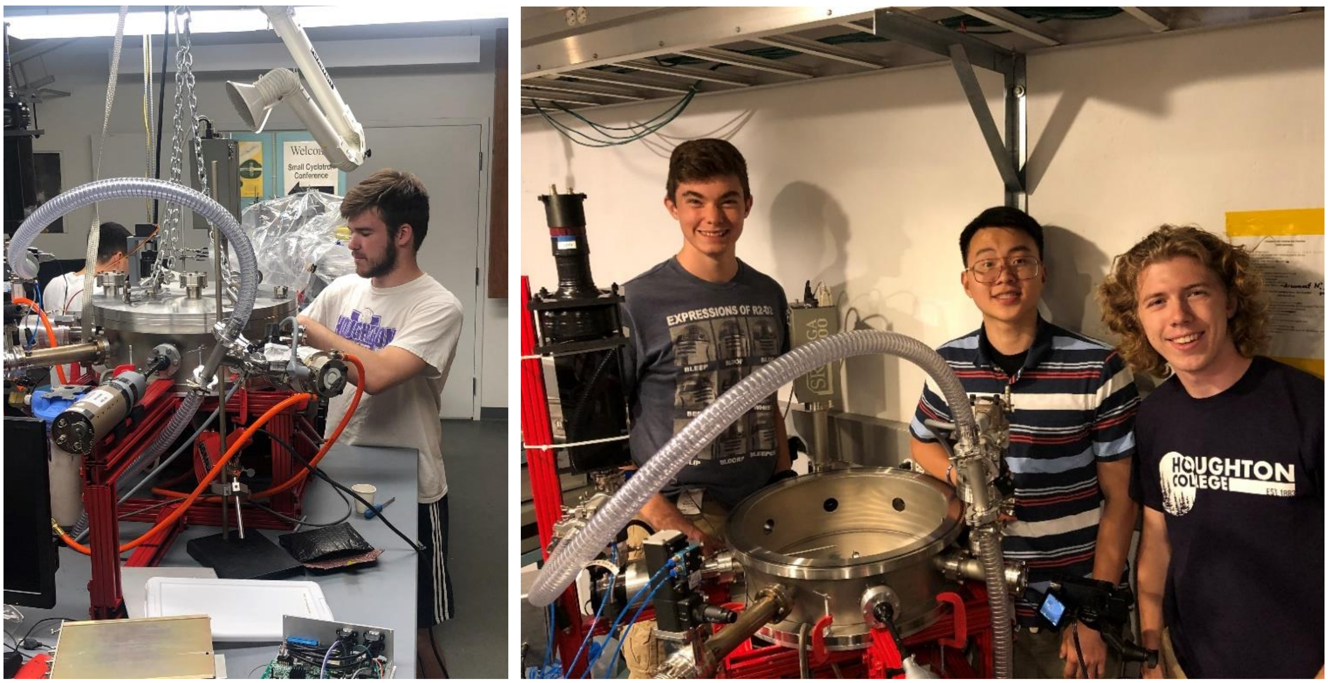

Figure 2. (Right) Houghton College student Andrew Martin preparing the test chamber for the 2022 trip to SUNY Geneseo. (Right) Andrew Hotchkiss, Chunsun Lei and Adam Brown (left-to-right) setting up the test chamber on the 30R beam line of the SUNY Geneseo Pelletron.

A. The ^{65}Cu(d,p)^{66}Cu and ^{19}F(d,p)^{20}F Measurements (2021)

Experimental Setup

Since the 2021 report [22] was due before the experiment was completed, it included a description of the setup but none of the results of the measurements. For that reason, only a brief summary of the setup will be given here, followed by a more detailed description of the not previously reported results.

A stainless-steel test chamber [13], approximately 50.8 cm (20 in.) diameter and 15.24 cm (6 in.) high was attached to the downstream side of the 30R beam line scattering chamber on the SUNY Geneseo 1.7 MV tandem Pelletron accelerator. The chamber was evacuated by a Pfeiffer Balzers TPH-062 Turbo Pump, and the pressure monitored using a Duniway I-100-K ion gauge, a Granville-Phillips Convectron convection gauge, and an SRS RGA100 residual gas analyzer.

Targets for the ^{65}Cu(d,p)^{66}Cu experiment were created [23] by electroplating copper onto a 0.05 mm thick tungsten ribbon approximately 6.5 x 12.5 mm. The ribbon was attached across the thick copper electrodes that were attached to an electrical feedthrough on the top chamber lid, positioning the copper in the center of the chamber. For measurements using the ^{19}F(d,p)^{20}F reaction, thin Teflon tape was wrapped around the tungsten ribbon and held in place with wire. A relay circuit allowed approximately 100 A to flow through the tungsten ribbon from a 12 V automobile battery, heating the ribbon to as high as 1450 °C. An automated rotating arm could be used to position an aluminum "shield" between the ribbon and the detector, and was used, for certain experiments, to stop radioactive material coming off the ribbon from reaching the detector. It then moved the material as far away as possible from the detector.

The getter trap detector [22] was a 1 mm thick, 9.5 mm (3/8 inch) diameter fast EJ-212 scintillator optically coupled using EJ-500 optical epoxy to a 15 mm long, 10 mm diameter cylinder of slow EJ-240 scintillator. The scintillator was glued to a 45.9 cm long, 10.1 mm diameter glass optical fiber lightguide using EJ-500 optical epoxy. The other end of the glass rod was pressed firmly against a Burle 7585 phototube and optically coupled with EJ-550 optical silicone grease. The glass lightguide passed through a vacuum feedthrough to position the detector approximately 3 cm from the center of the chamber.

The turbopump trap [14, 19] is a hollow 246 x 84 x 84 mm rectangular prism made of 18 mm thick EJ-240 slow plastic scintillator, the inside of which is lined with 1 mm thick EJ-212 fast plastic scintillator. The light released by the scintillator was collected by a 130 mm (5-inch) phototube attached to one end. The other end of the hollow box was attached to the foreline port of an Edwards EXT70H Turbo pump, which trapped gas molecules traveling down a 6.35 mm (0.25 inch) OD diameter, 0.254 mm (0.010 inch) wall thickness 316L stainless steel tube that reached to approximately 3 cm from the center of the chamber.

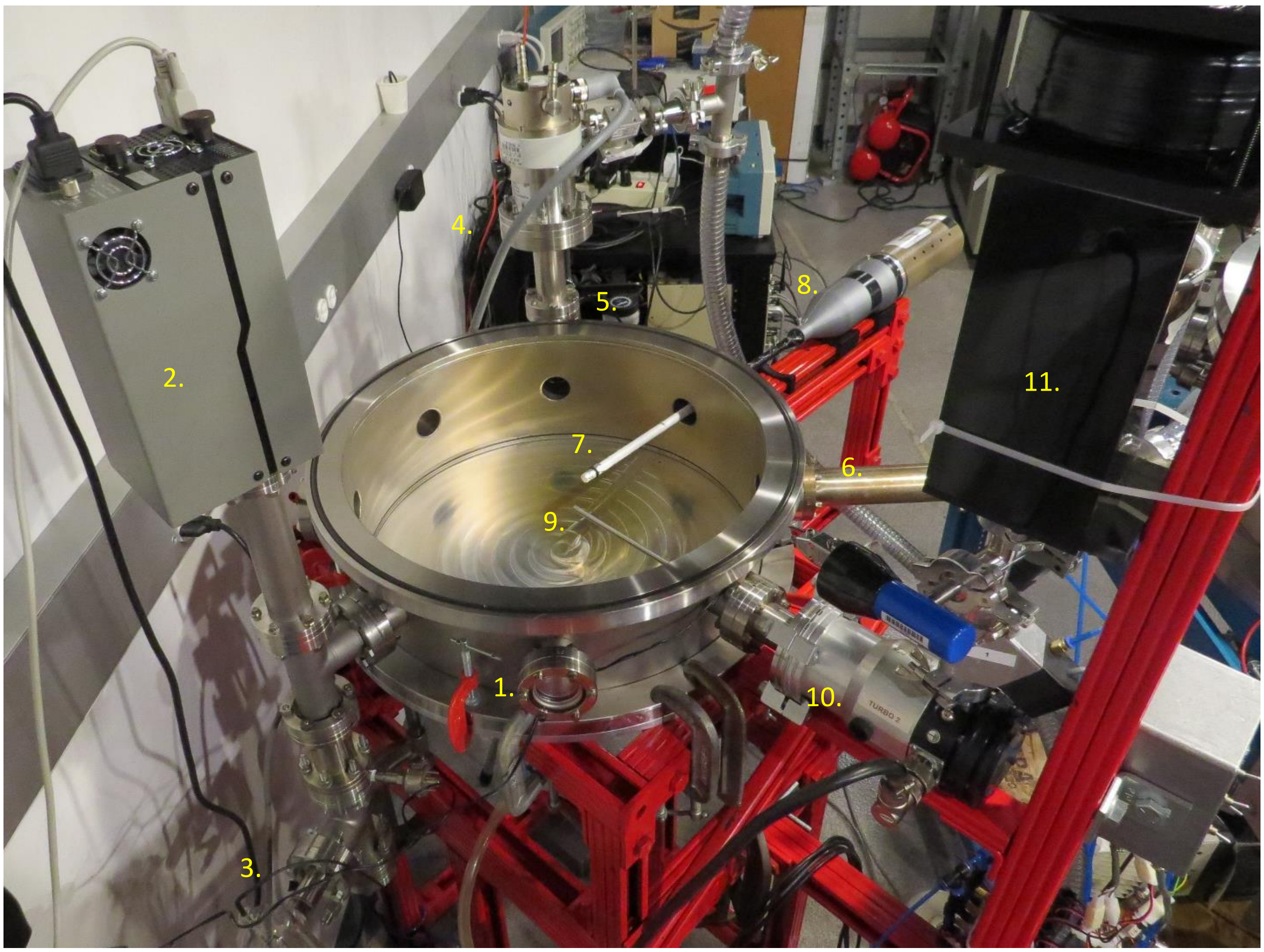

Figure 3. Photograph of the test chamber and associated apparatus attached to the 30R scattering chamber on the SUNY Geneseo Pelletron in 2022. The two viewports (1 and 5) allow a camera to see the target foil or the temperature to be measured with the pyrometer. The RGA (2), ion gauge and thermocouple gauge (3) allow the pressure and composition of the gas in the chamber to be determined. The chamber turbopump (4) evacuates the chamber. The deuteron beam enters from the accelerator beamline (6), striking the target which would be located at the center of the chamber. After the target foil is heated by discharging the capacitors through it, the vaporized target material sticks to the foil on the end of the getter detector (7). Light travels down the glass light guide to the phototube (8). The gas could also enter the collection tube (9) and be trapped by the turbopump (10) inside the 4π detector (11).

Signals from the detectors were processed by NIM electronics [22] to separate the slow and fast components using fast linear gates. The resulting separate fast and slow analog pulses were then digitized using a Skutek FemtoDAQ digitizer and stored for later analysis.

In each of the counting experiments, an approximately 30-100 nA beam of 1.514 MeV deuterons produced by the SUNY Geneseo Pelletron was allowed to strike the target. To align the deuteron beam, a quartz window was clipped to the copper plated tungsten ribbon and viewed with a camera through a chamber viewport. The quartz glowed when struck by the beam, so the beam could be steered and readjusted until the beam spot was over the center of the tungsten ribbon.

Once the beam was hitting the center of the tungsten ribbon, the chamber was filled with dry nitrogen and the exploding wire device was taken out so the quartz could be removed. The target with exposed the copper film exposed was inserted back into the chamber, which was re-evacuated to a pressure of about 5×10^{-6} Torr. The accelerator gate valve was opened, and the deuteron beam was allowed to strike the copper for 30 minutes (^{66}Cu half-life is 5.15 min) or the Teflon film for 90 seconds (^{20}F half-life is 11.07 seconds). After this interval, beam was stopped by inserting an upstream faraday cup.

A C++ analysis code written using the ROOT analysis framework [24] was used to identify beta decay events, and for these events plot the decay curve. Figure 4 shows a typical 2D histogram from the getter detector, with the quadrangle indicating good beta events. The decay curve was also integrated to produce a growth curve, which was fitted using MINUIT [25]. In most cases the growth curve was fit to extract he decay constant, background, and total number of detected decays. However, for the ^{19}F(d,p)^{20}F experiment, when the count rate was high enough that the FemtoDAQ memory needed to be read out during the relatively short counting interval, resulting in a dead gap, the decay curve was fit.

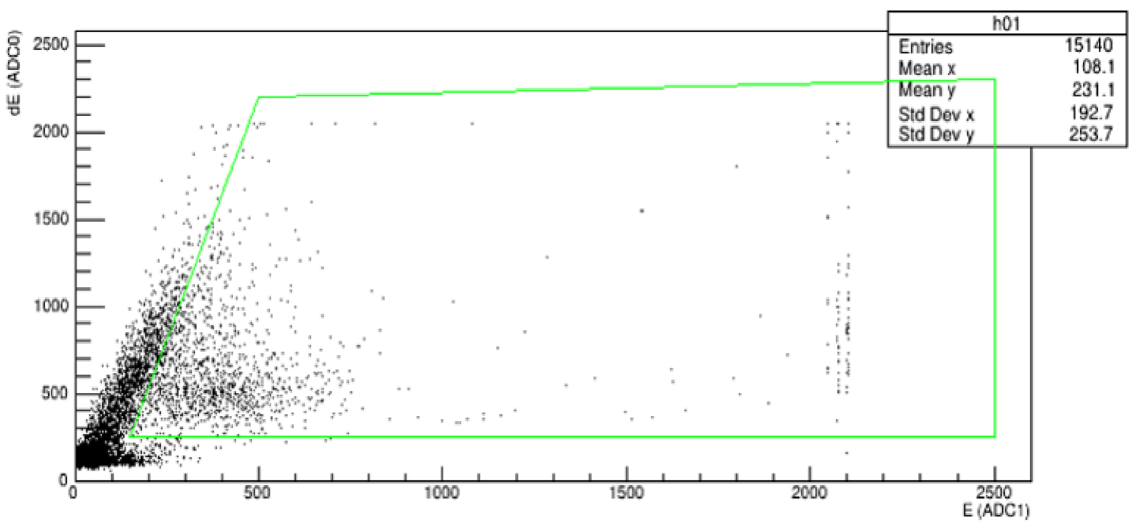

Figure 4. A typical 2D histogram created using events from the getter defector from ^{66}Cu on the getter foil. Events inside the green quadrilateral were considered to be "good beta events" and included in the decay curve.

Detecting ^{66}Cu in situ on the tungsten foil from ^{65}Cu(d,p)^{66}Cu

In order to determine the amount of ^{66}Cu produced in the copper film, the incident deuteron beam was allowed to strike the film, but the film was not evaporated. Rather, the getter detector was allowed to count the ^{66}Cu decays in situ. Figure 5 shows the decay and growth curves obtained.

Detecting ^{20}F in situ on the tungsten foil from ^{19}F(d,p)^{20}F

A similar ^{20}F experiment was carried out with Teflon tape wrapped around the tungsten ribbon and activated by the deuteron beam. Because of safety concerns at the time, the Teflon was never heated, but the getter detector was nevertheless used to identify ^{20}F in situ.

The results from this test are shown in Figure 6. Since the half-life of ^{20}F was much shorter than that of ^{66}Cu, the FemtoDAQ could not keep up with the higher count rate, leaving "gaps" in the counts vs. time histogram when the Beaglebone microcontroller in the FemtoDAQ was reading out the FPGA. In the growth curve these gaps integrated into horizontal lines, making it impossible to fit a growth curve. Instead, the previously measured half-life of 11.07 s for ^{20}F was used as a fixed parameter in the decay curve fit, shown in red.

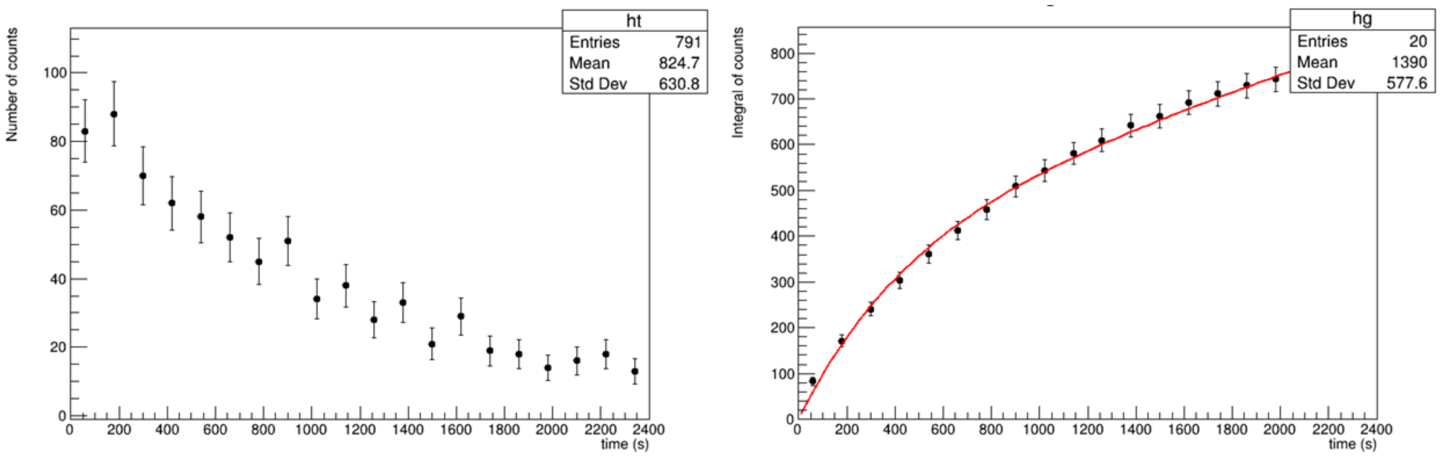

Figure 5. Measured in-situ decay (left) and integrated growth (right) curves for ^{66}Cu in the unevaporated film using the getter detector, in 2-minute time bins. The fit, shown in red, gave 401 ± 71 decays with a half-life of 5.23 ± 1.15 min.

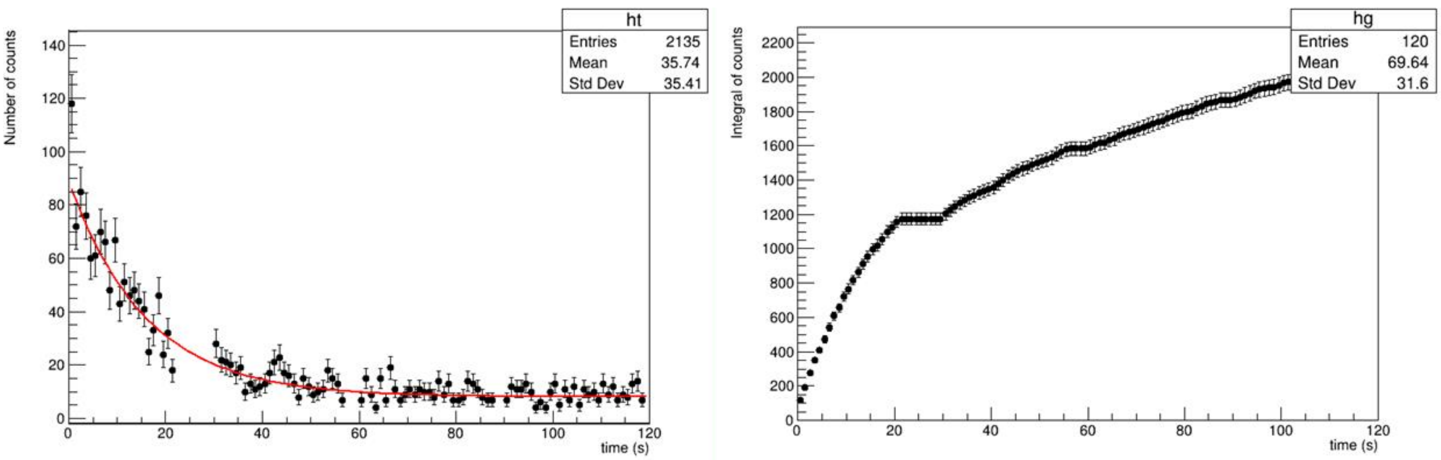

Figure 6. Measured in-situ decay (left) and integrated growth (right) curves for ^{20}F in the unevaporated Teflon tape using the getter detector, in 1 sec time bins. The fit, shown in red, gave the initial rate of $\mathbf{80.8 \pm 2.9}$ decays/sec.

Exploding wire experiment to detect ^{66}Cu on the getter foil

One concern with this experiment was that not all the copper would evaporate off the tungsten. This could result in decays of residual ^{66}Cu on the tungsten being counted by the getter detector in addition to any trapped ^{66}Cu stuck on the getter itself. To address this, two thicknesses of electroplated copper were used in the hope that if the thicker film did not completely evaporate, the thinner on would. On the other hand, the thicker film should contain more ^{66}Cu, which would result in a better signal if it all came off. For this reason, the thicker 25 μm layer was used as a first attempt to maximize the amount of ^{66}Cu, then a thinner 11 μm layer was used to reduce the amount of copper that might remain on the tungsten. The 25 μm film was electroplated across the entire tungsten ribbon on both sides and the 11 μm film was electroplated only in a square in the center of one side of the tungsten ribbon.

The results for both the 11 μm and 25 μm thick evaporated copper films are shown in Figure 7. In both cases the exponential nature of the decay curve is clear, and a fit to the growth curve yields a half-life that is within error bars of the previously measured value, indicating that ^{66}Cu did indeed evaporate and stick to the getter foil. Moreover, after the experiment, copper could be seen coating the getter foil on the end of the getter detector.

Rotating Shield

The question of whether or not there was residual copper on the tungsten after the tungsten foil was heated the was addressed more fully with an experiment involving the rotating shield. The shield, with was attached to a rotating arm, was used to “catch” the evaporating copper and then move it to the other side of the vacuum chamber from the getter detector. An 11 μm thick layer of copper was activated by the deuteron beam and evaporated onto the shield, directly between the target foil and the getter detector. The shield was then rotated away and the getter detector counted the decays from any residual ^{66}Cu left on the tungsten, although it could conceivably also detect ^{66}Cu stuck on other nearby surfaces, if any.

The results from the rotating shield experiment are shown below in Figure 8. As expected, the decay curve showed much fewer decays, since presumably there was no ^{66}Cu stuck on the getter foil. To determine the number of ^{66}Cu decays that were counted, however, the decay and growth curves were fit, with fixed half-life parameter of 5.12 minutes, to obtain 109 ± 21 (decay curve fit) or 134 ± 14 (growth curve fit). Compare this to the 4171 ± 249 decays using the 11 μm thick copper film when copper was allowed to reach the getter. Moreover, after each exploding wire experiment, there appeared to be no copper stuck on the tungsten ribbons, as shown in Figure 35 with tungsten ribbons from two different exploding wire experiments.

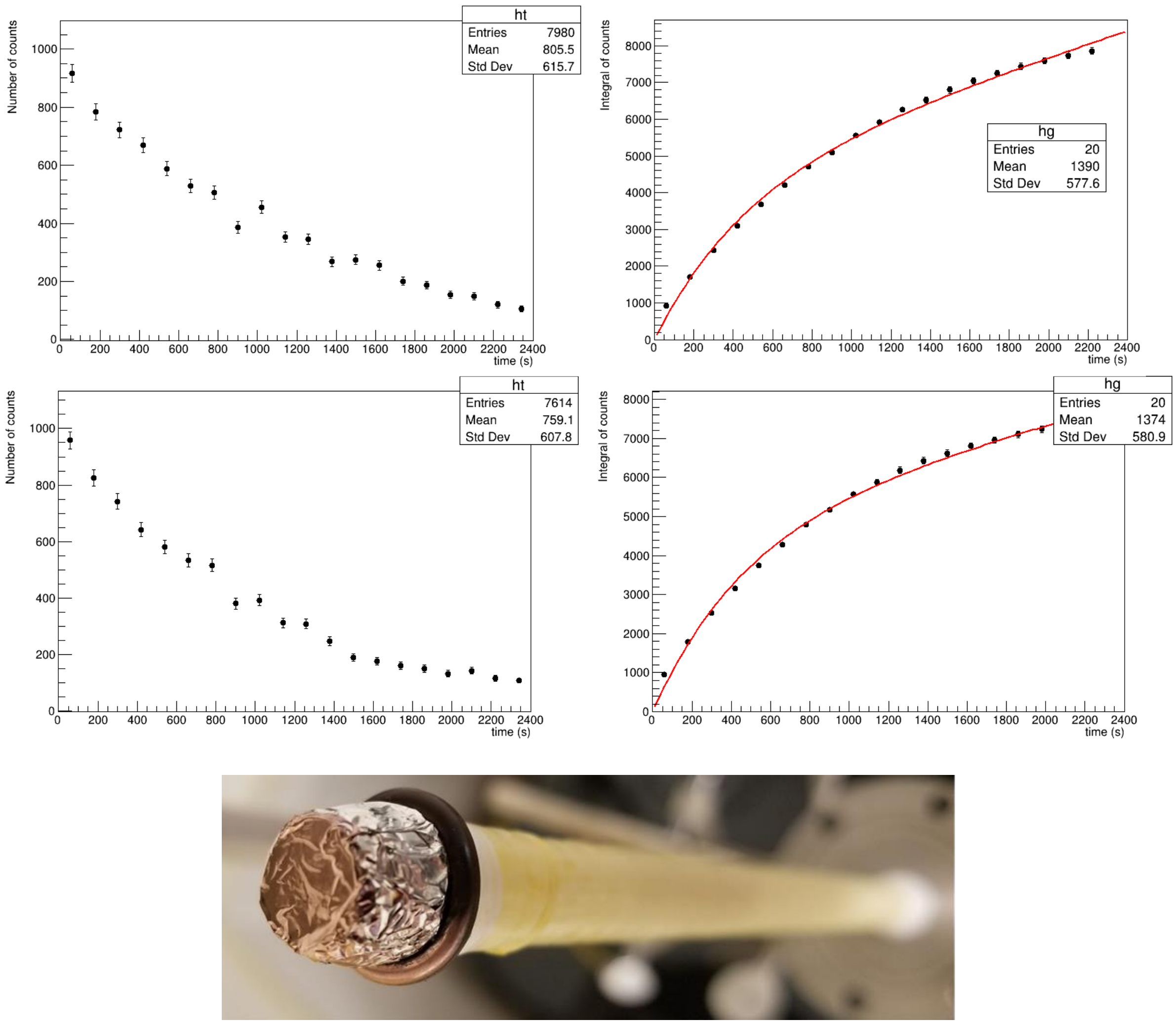

Figure 7. Results from evaporating 11 μm (top row) and 25 μm (middle row) thick copper onto the getter detector, counting ^{66}Cu beta decays to produce a decay curve (left) and integrating the decay curve to produce a growth curve (right) with 2 min time bins. Fitting the growth curves gave 4171 ± 249 decays with a half-life of 5.38 ± 0.38 min for the 11 μm thick foil and 4635 ± 244 decays with a half-life of 5.40 ± 0.34 min for the 25 μm thick foil. (Bottom) Photograph showing copper coating the getter foil at the end of the experiment.

Turbopump trap experiment

For the turbopump trap, a slightly modified procedure was used. Once the chamber was evacuated, the copper was irradiated for 30 minutes, the upstream Faraday cup was inserted, and the accelerator gate valve was closed. Next, a remote-controlled pneumatic valve was closed between the turbopump outlet port and the foreline. Another pneumatic valve was then opened, creating a pathway between the turbopump outlet and the 4π detector. The tungsten was heated for 10 seconds, evaporating the copper. The valve remained open for an additional 10 seconds, then closed, and data were collected for 40 minutes.

The results are shown in Figure 9. Within the first few minutes, it was apparent that the turbopump detector was only detecting a constant background of approximately 200 counts per time bin. The accelerator control room asked to briefly take out the Faraday cup at around 800 seconds, which led to higher background counts at around 800 sec. Regardless, an attempt was made to fit a growth curve, with a fixed half-life of 5.12 minutes. It is believed that the reason ^{66}Cu beta decay events were not detected is because all of the copper stuck to the aluminum collection tube and not reached the detector, a not unexpected result since this detector was designed for inert gasses. This idea is borne out by the photograph showing the end of the collection tube with a copper coating on the rim.

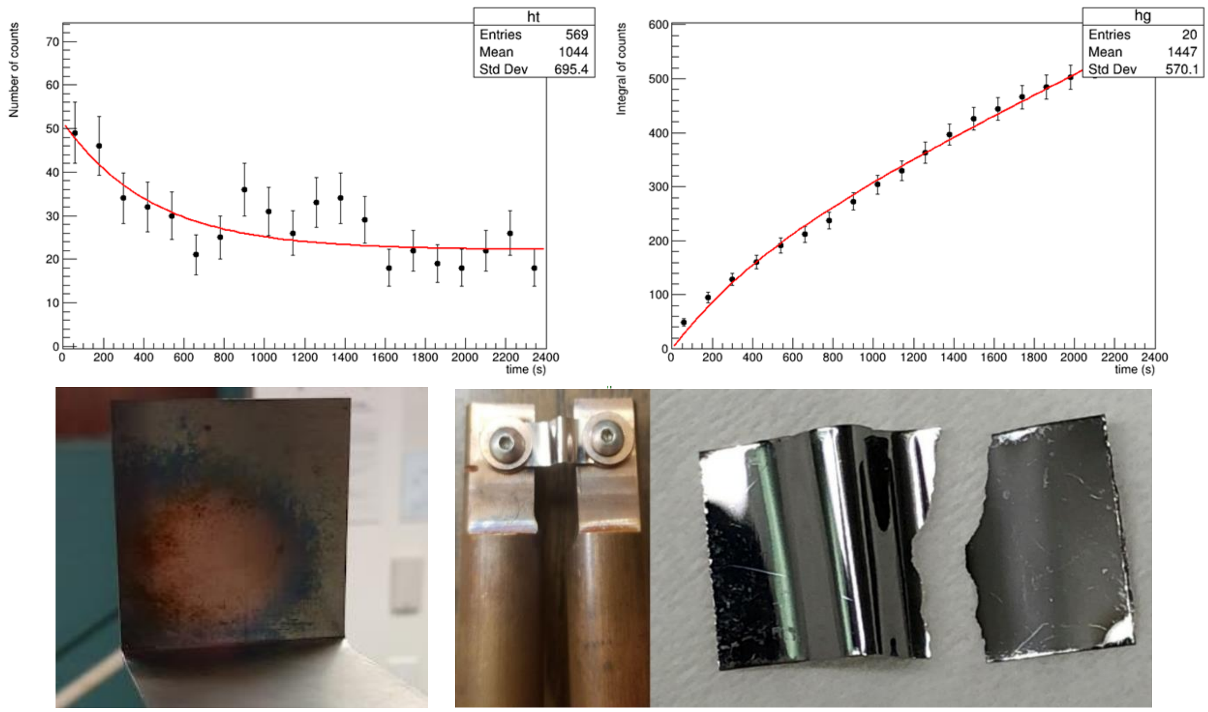

Figure 8. Results from the rotating shield experiment. The evaporating copper was caught by the rotating shield before it could reach the getter detector. The shield rotated 120° to the opposite side of the chamber. The getter detector was then used to find any residual ^{66}Cu on the tungsten or elsewhere nearby in the chamber. Decay (top left) and growth (top right) curve fits were made with fixed 5.12-minute half-life to determine the total amount of residual ^{66}Cu detected was only 109 $\pm$ 21 (decay curve fit) or 134 $\pm$ 14 (growth curve fit). Photograph showing the copper coating on the rotating shield after the experiment (bottom left) and the copper film has disappeared from the tungsten foil (bottom right).

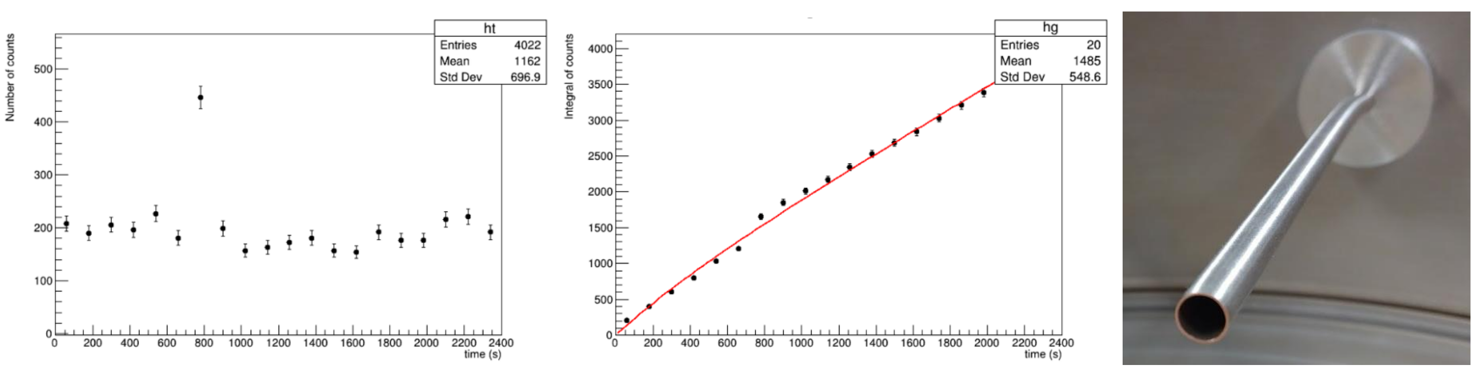

Figure 9. Results from evaporating an 11 μm thick copper film and attempting to trap it with the 4π detector. The resulting decay curve (left) was integrated to give the growth curve (center) with 2 min time bins. Fitting the growth curve gave 367 $\pm$ 33 decays with the half-life set to be a fixed parameter at 5.12 min. (Right) Photograph showing copper coating the end of the collection tube at the end of the experiment.

B. The $^{7}Li(d,p)^{8}Li$ Measurements (2022)

During the summer an attempt was made to evaporate and trap ^{8}Li from the tungsten foil. Since most of the apparatus was the same as the ^{66}Cu and ^{20}F experiments from 2021 [22], only items that are new are described below.

Lithium Deposition Chamber

In order to create thin lithium films on the tungsten foil, a vacuum deposition chamber was designed and built. As seen in Figure 10, it consists of a cylindrical vacuum chamber, 95 mm diameter and 265 mm high, with five conflat flange ports, evacuated to about 10^{-6} Torr by a 2-inch diffusion pump and a Varian Tri-Scroll forepump. The pumps are connected through a series of valves that allow the chamber to be isolated and let back up to one atmosphere while keeping the diffusion pump hot and under vacuum. A second forepump (ULVAC G-50D oil rotary pump) can be used to evacuate the chamber before re-opening the valve to the diffusion pump. Inside the chamber is "boat" used to heat the lithium pellets and a "house" the holds the tungsten foil. These are supported by a two-conductor 2.75-inch conflat power feedthrough with ¼ inch rod electrodes. This feedthrough is attached to the side 6-inch conflat flange, which also supports two 1.33-inch conflat thermocouple feedthroughs for measuring the temperature of the boat and house. The top 6-inch conflat flange has an adapter to a KF-40 flange, which is used for inserting the tungsten foil. The bottom 6-inch flange is a viewport that is used for observing the bottom of the boat. The two remaining 2.75-inch conflat ports are used for pumping the air out of the chamber and for a side viewport used when positioning the tungsten substrate foil on the top of the house. Surrounding the deposition chamber is a glove bag filled with argon gas, to allow the lithium films to be removed and handled. The pumps are located outside the glove bag, since the diffusion pump needs to be air cooled.

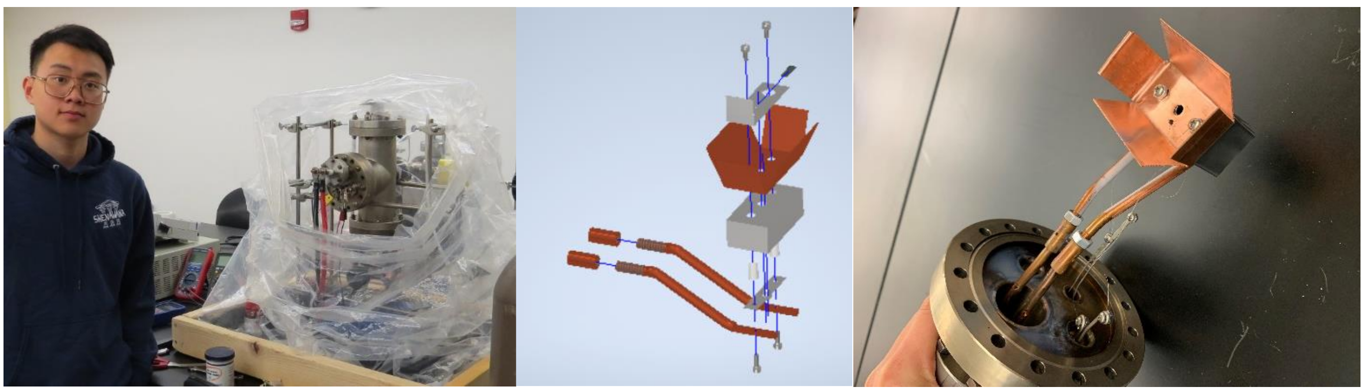

Figure 10. (Left) Houghton student Chunsun Lei with the lithium deposition chamber that he is using to produce the thin lithium films for this experiment. (Center) An exploded 3D CAD drawing showing how the "boat", used to heat the lithium pellets, is attached to and supported by the power feedthrough rods and how the "house" supports the tungsten film and contains the lithium vapor. (Right) A photograph of the entire assembly.

The "boat" is a 50 mm long by 15 mm wide by 0.05 mm thick strip of 321 stainless steel, with an approximately 15 mm diameter divot in its center. It is attached to the copper rods using 4-40 screws, with threaded ceramic insulators holding it tightly down for good electrical contact. On top of the ceramic insulator a 321 stainless steel "house" contains the lithium vapor and keeps it, as much as possible, from depositing on other surfaces in the vacuum chamber. Attached on top of the house is a copper heat sink and radiator, whose purpose is to keep the house and the tungsten foil below the lithium melting point. A 6 mm dimeter hole in the top of the "house" and the copper radiator allows lithium atoms to reach the tungsten foil substrate, which is held in a special stainless-steel holder that can be easily lowered through the top KF-40 port and positions the foil above the hole.

In order to create the film, argon gas is used to flush the air out of the glove bag and fill it, so that the oxygen content, measured with a Seesii 4 Gas Monitor, is less than 4% and the humidity is below about 20%. Approximately 0.038 g of lithium, in the form of small pellets, are inserted into and allowed to slide down an aluminum tube that reaches from the top port, through the hole in the "house", and down to the divot in the "boat". The tube is removed and the chamber closed and evacuated to the 10^{-5} torr pressure range. Electrical current from a Mastech HY 1550EX high current power supply is allowed to flow through the boat, slowly increasing to about 20 A. At 20 A, the "boat" temperature equilibrates at about 400°C, and the "house" is at about 100°C, as measured with two Type-K (Chromel/Alumel) thermocouples attached with Rutland Products Furnace Cement. The glowing stainless steel "boat" can be viewed from below using a SVPRO 1080P HD optical zoom camera. Once the lithium melts at approximately 180°C, its temperature will not rise until is all vaporized. This results in a dark circle in the camera view where the "boat" is not glowing, as shown in Figure 11. As the lithium evaporates over a period of 11 or 12 minutes, the dark circle slowly shrinks until all the lithium is evaporated, and the circle disappears.

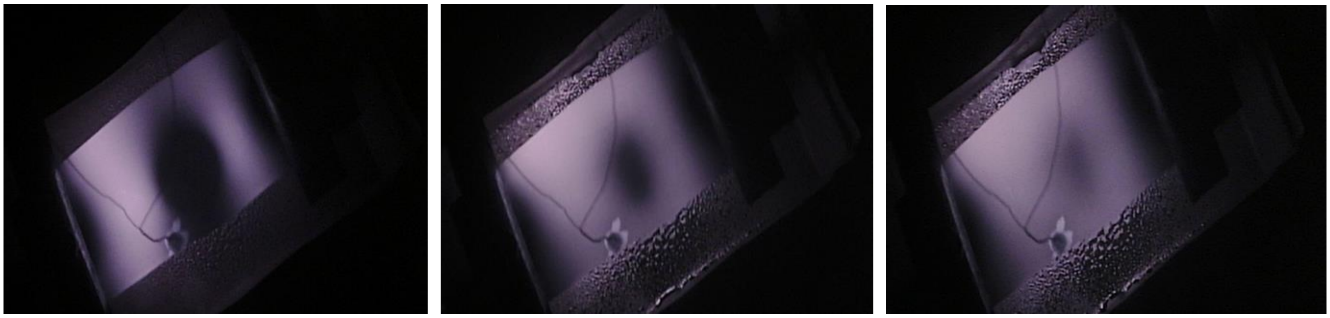

Figure 11. Photographs of the underside of the "boat" showing the cool, dark circle that is created by the evaporating liquid lithium, at the start before any lithium has evaporated (left), when it is halfway gone (center), and when it is completely evaporated (right). Also visible is the thermocouple attached to the boat.

Once all of the lithium is evaporated, the tungsten foil is removed from the vacuum chamber into the argon filled glove bag. Its thickness, with is typically in the range or 20 to 100 μm, is measured using a micrometer with special micrometer tips.

An evacuated holder is used to store and transport the films after they have been produced. A 2.75-inch conflat "tee" is attached, through a valve, to the ULVAC forepump which keeps the pressure inside around 30 mT. On the other end of the tee a conflat-to-quick flange adapter allows films to be easily inserted into the tee, and a thermocouple pressure gauge to monitor the storage pressure, especially when in-transit and not connected to the vacuum pump.

Rotary Target Holder

A special target holder was made using differentially pumped rotary feedthrough with a four-conductor electrical power feedthrough attached. This allows three different tungsten foils and a quartz viewer for aiming the beam to be in the vacuum chamber, so that several experiments can be performed before the vacuum system needs to be opened and new targets inserted, a time-consuming process. This is an improvement over the 2021 experiments in which the vacuum system had to be opened to insert the quartz or a target every single time.

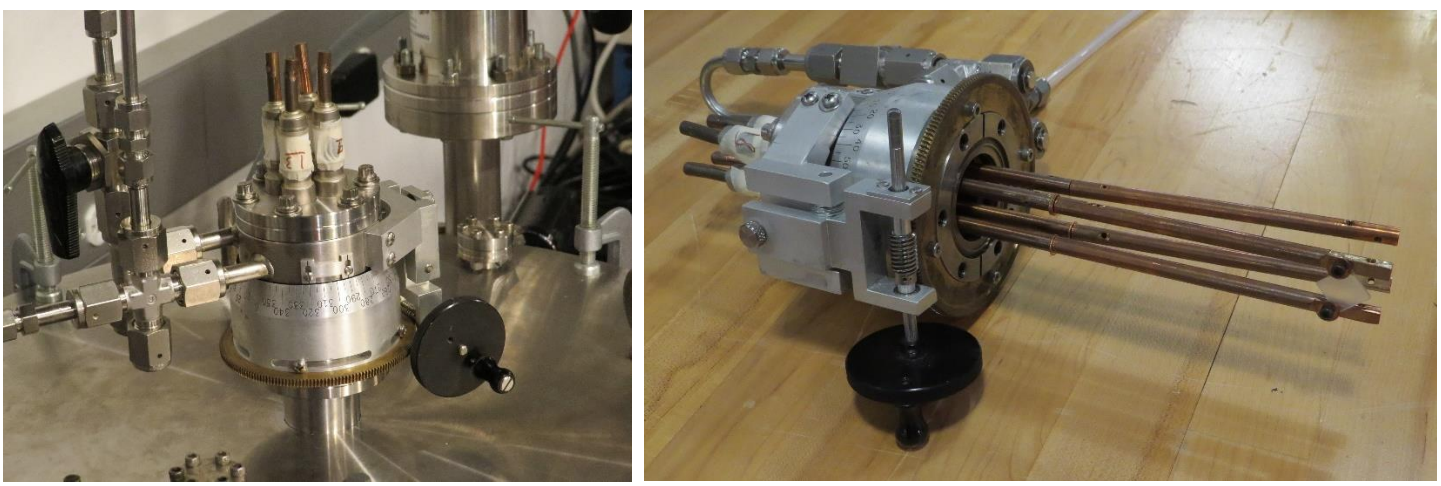

Figure 12. Photographs of the differentially pumped rotary feedthrough attached to the test chamber (left) and the copper rod electrodes attached to the electrical feedthrough on the rotary feedthrough (right) with a quartz viewer attached for finding the beam spot.

Experiment control and data acquisition

Many improvements were made to the controls for the experiment and to the data acquisition system between 2021 and 2022. The 2020 OMEGA ride-along experiment made it very obvious that the FemtoDAQ acquisition system did not have enough memory and transferred data too slowly for our application. Moreover, given the small number of laser shots, it would be very advantageous to record not just the digitized integrated charge in a "fast" and "slow" time window from the phoswich detector phototube, but to actually record the entire waveform for each pulse. In order to address these issues, during the summer of 2022 the FemtoDAQ was replaced with a CAEN N6730SB digitizer [26]. This new digitizer is capable of sampling eight 250 MHz-bandwidth inputs every 2 ns with 14-bit resolution. It can store 5.12 megasamples for each channel and can transfer data to another computer over USB at a rate of 30 MB/s -- which means it should be able to handle the count rates encountered in the OMEGA ride along experiment. For the 2022 experiments, it was configured to sample and record the waveform every 2 ns for an 800 ns period starting shortly before the trigger.

The CAEN digitizer is being read out using an Atomic Pi [27], a single board computer with a 1.92 GHz Intel Atom x5-Z8350 quad core processor with 2GB DDR3L-1600 RAM and built-in16GB eMMC flash memory. The Atomic Pi was selected because the CAEN-provided software libraries for its digitizers only run on Intel processors. A Raspberry Pi 4B [28] single board computer was used to control the experiment. Both computers were mounted in NIM modules located in a NIM bin near the target chamber. Remote sessions over an ethernet network allow another computer, located in the "counting station" in the hallway outside the accelerator hall, to control the experiment and save and analyze the collected data.

Since the half-life of ^{8}Li is only 840 ms, all aspects of the experiment needed to be controlled by the Raspberry Pi 4 computer. Figure 13 shows the circuit used to control the various valves and the electrometer used to integrate the total charge from the beam striking the target. The CAEN waveform digitizer is also enabled by a signal from the Raspberry Pi. Finally, Figure 15 shows the SCR circuit used to discharge the capacitor when it receives a signal from the Raspberry Pi.

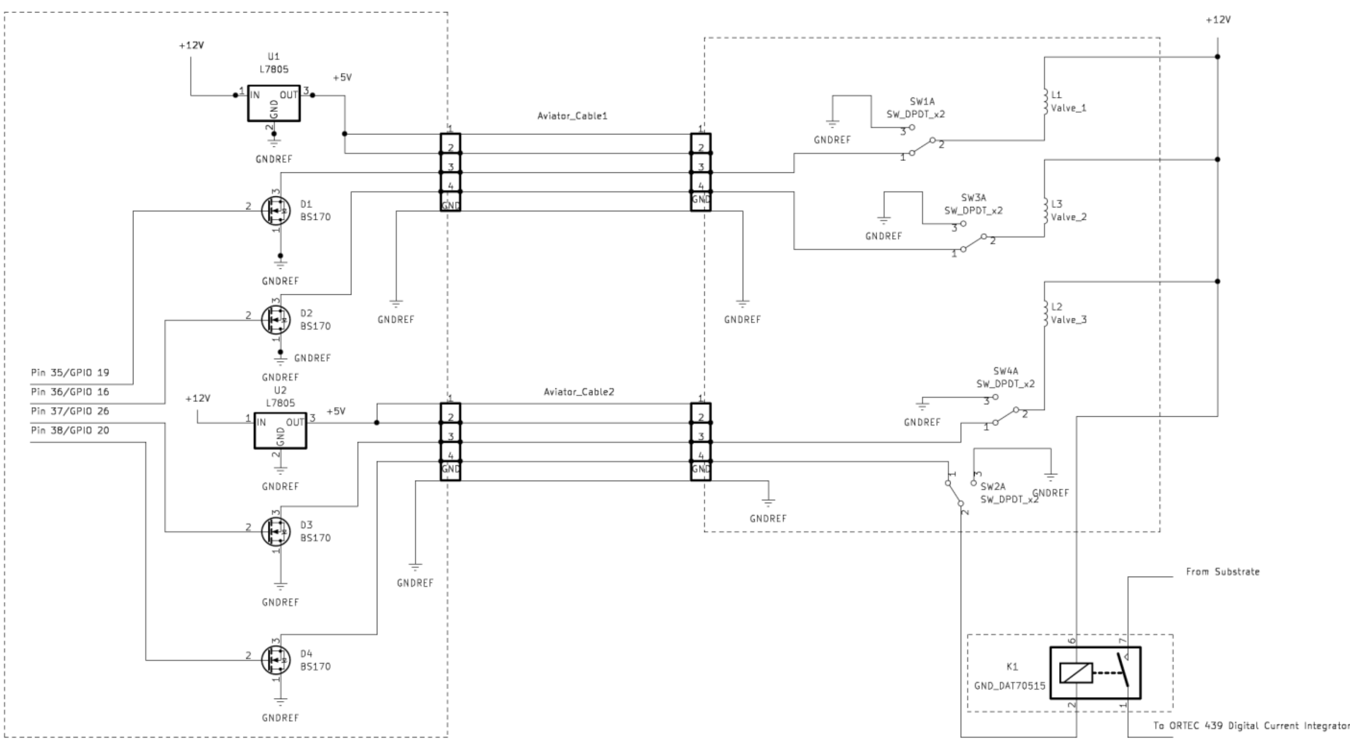

Figure 13. The Raspberry Pi computer controls all aspects of the experiment including the gate valve between the test chamber and the beamline and the foreline valves in the turbopump trap detector. An electrometer is used to integrate the total charge striking the target. The electrometer is removed from the circuit by a relay just before the capacitors are discharged.

The timing for the signals is as follows. First, the Faraday cup is removed, allowing the deuteron beam to strike the lithium on the tungsten foil. The radiation produced by this creates a high count rate in the NaI detector, causing the output of the NIM latch circuit to latch high. The CAEN digitizer program is started, and waits for a signal from the Raspberry Pi before beginning to record events. Next, a python program on the Raspberry Pi is started, which starts the CAEN digitizer and connects the electrometer to begin integrating the total beam charge on the target.

After 10 seconds, the electrometer is disconnected, and the Raspberry Pi begins looking for the falling edge from the latch circuit, indicating the Faraday cup has been inserted to cut off the beam. When it detects the falling edge, it closes the pneumatic valve between the test chamber and the accelerator beamline and disables the CAEN digitizer. It waits for 2 ms, discharges the capacitor through the tungsten foil and then re-enables the CAEN digitizer for 10 seconds. Disabling and reenabling the digitizer allows the timing of cutting off the beam and discharging the capacitors to be recorded in the data stream.

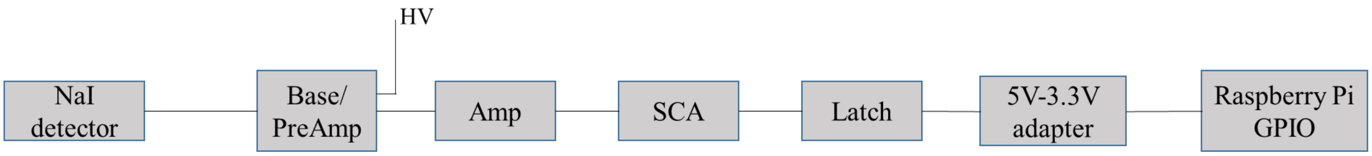

Figure 14. Block diagram of NIM latch circuit used to determine when the beam was cut off by the Faraday cup. Each pulse from the NaI detector generates a digital high output from the latch circuit lasting for approximately 1 ms. If another NaI pulse arrives before the end of the 1 ms period, it restarts, setting the output high for the next 1 ms. If another pulse does not arrive in time because the Faraday cup was inserted, shutting off the beam, then the falling edge of the digital output signals to the Raspberry Pi that the cup was inserted.

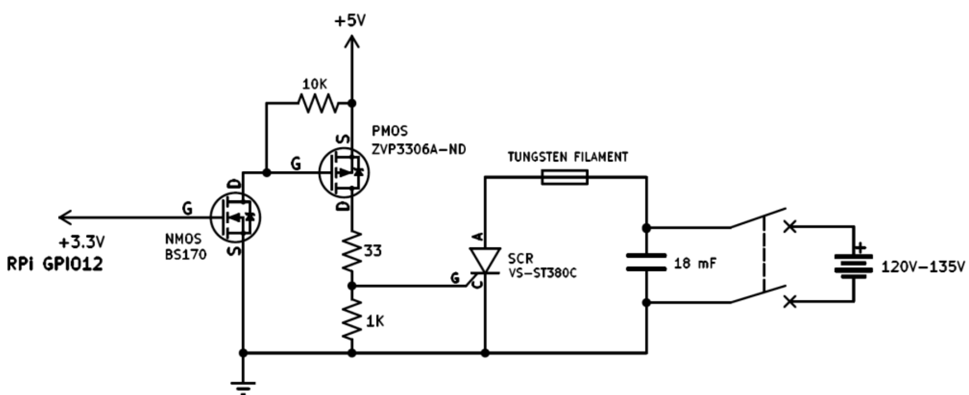

Figure 15. The SCR trigger circuit used to discharge the capacitors. A 3.3 V signal from the GPIO port of the Raspberry Pi turns on the N-Channel MOSFET, which then turns on the P-channel MOSFET causing current to flow into the gate of the SCR turning it on and discharging the capacitor.

Preliminary 2022 Results

This report was written while the experiment was still underway. Figure 16 shows the first measurement using a lithium film target. The phototube gain was reduced by lowering the voltage to -1900V. A 2D histogram made using a ^{207}Bi source (top left), which emits monoenergetic electrons at approximately 1 MeV and 0.5 MeV, as well as a beta spectrum, shows the expected shape with a conspicuous group of events due to 1 MeV electrons. Events recorded when the deuteron beam was hitting the lithium (top right) show a broad band in E with approximately constant dE where electrons are expected, but extending to much higher energies than ^{207}Bi since the beta spectrum extends up to about 13 MeV. The spectrum does not extend as far as otherwise expected, however, since electrons with energies above about 3.5 MeV punch through the scintillator. On this histogram, there is also a band where the dE signal is large but there was no E signal. Preliminary analysis indicates these events may possibly be due to protons (~5 MeV) and/or alpha particles (~10 MeV) from the ^{6}Li(d,p)^{7}li and ^{6}Li(d,α)^{4}He reactions, respectively.

For the data collected after the lithium was activated and the capacitors were discharged, good electron events were selected by cutting on the 2D dE-E histogram based on the results obtained from using a ^{207}Bi beta source to estimate the location of electron events. A histogram the timestamps of these events yields the decay curve shown in Figure 17. Integrating this decay curve yields the growth curve, which was fit to obtain the half-life value of 845 $\pm$ 2 ms.

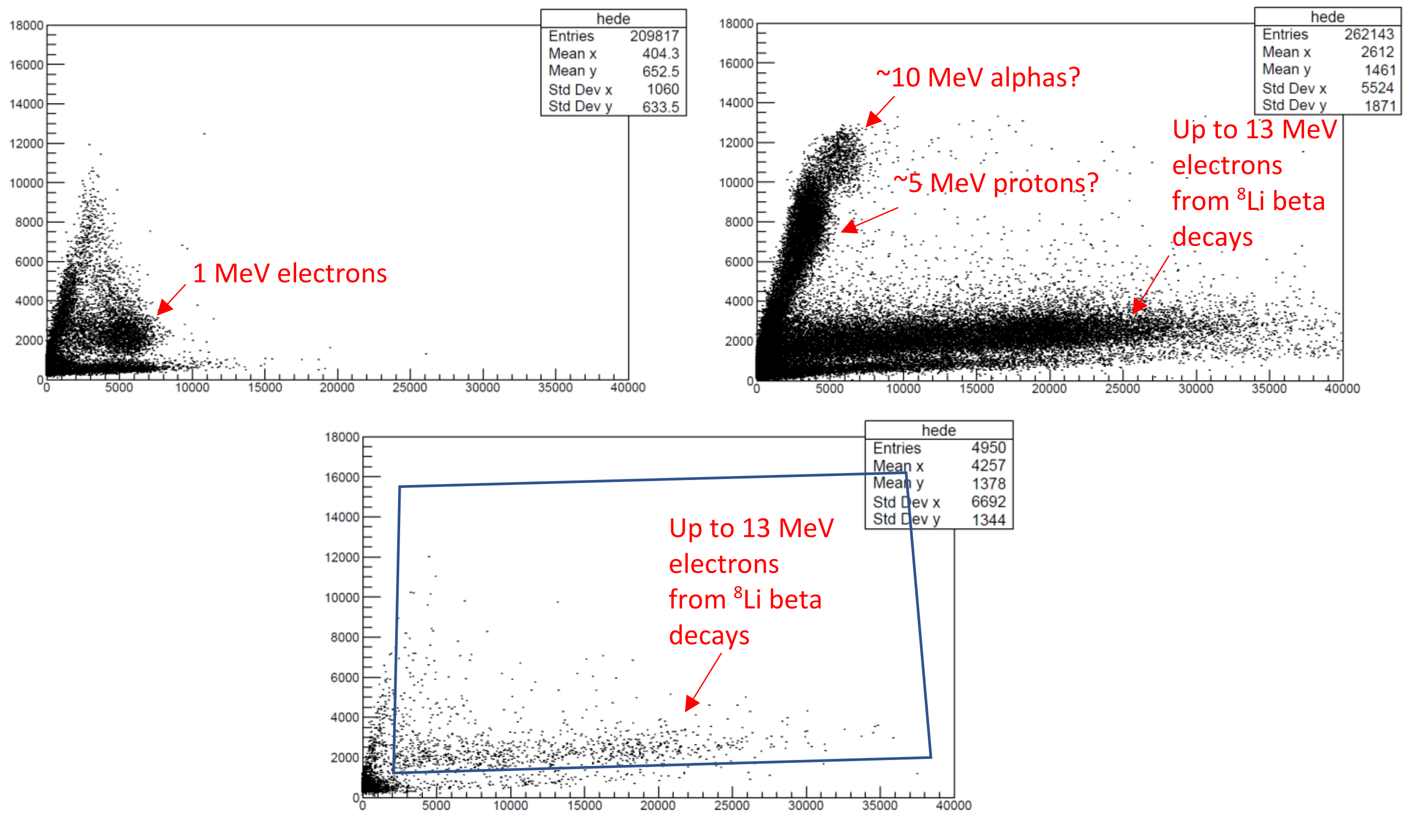

Figure 16. Getter phoswich detector 2D histograms with the fast component (mostly thin dE detector) on the vertical axis and the slow component (mostly thick E detector) on the horizontal, in arbitrary units, for the ^{207}Bi calibration source (top left), the deuteron beam striking the lithium target (top right) and the lithium on the getter detector after discharging the capacitor (bottom). Good beta events were selected (blue quadrangle) and their timestamps used to create a time spectrum.

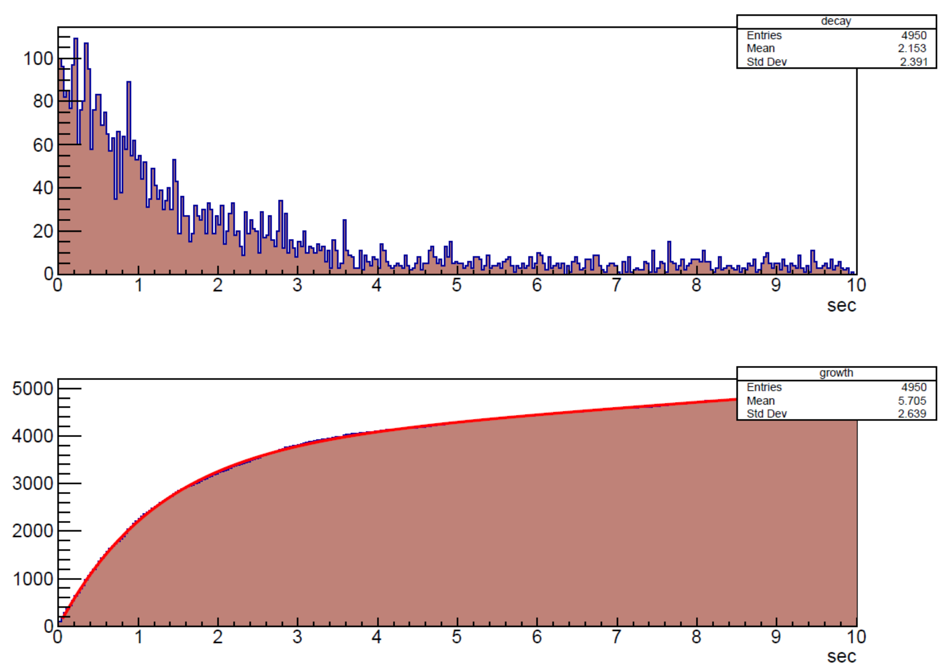

Figure 17. (Top) Histogram of good beta decay event timestamps after the capacitor was discharged (t=0). A decay curve is formed which was integrated to form a growth curve (bottom). A Minuet fit (red curve) of the function $\boldsymbol{A}\left(\mathbf{1}-\boldsymbol{e}^{-\boldsymbol{\lambda t}}\right)+\boldsymbol{Bt}$ yields a half-life of $\mathbf{845} \pm \mathbf{2}$ ms, which compares well with he previously published value of 840 ms.

III. Future Plans

The next steps currently being considered for this project, assuming continued success for the remaining experiments this summer, are the following:

1. **Geant4 simulation and validation.** In order to determine the trapping and detection efficiency, it is necessary to understand the intrinsic efficiency of the detectors. Tthe Geant4 simulation of our detectors created in 2020 will be used to calculate the efficiency, then the simulation predictions will be validated using radioactive sources, and finally used to calculate the efficiency for ^{8}Li. This plus the data we collect this summer will allow the fraction trapped and detected to be accurately determined.

2. **Another OMEGA ride-along experiment.** The 2020 ride-along experiment showed that the background in the getter detector, without the light guide, was low enough to do an ICF experiment using OMEGA, but the rate in the 4π detector was too high. It also showed the FemtoDAQ was too slow to handle the high count rates. In a future ride along experiment it would make sense to test the effect of shielding to reduce the background count rate in the 4π detector, the effect of including the lightguide on the getter detector, and the ability of the CAEN digitizer to keep up at high rates. Also, the decay of the background count rate after the laser shots seems to point toward ^{16}N and ^{26}Al* as possible culprits that we could try to mitigate.

3. **Test new FemtoDAQ+ digitizer.** As part of a new OMEGA ride along experiment, we would also like to carry out a head-to-head test of the CAEN digitizer with the newly redesigned FemtoDAQ+ digitizer.

4. **Increase lightguide transmission.** Experiments with fiber optic light guides to replace the glass optical rod will continue. The cladded glass light guide is better than the other solid rod materials tested, such as acrylic and polycarbonate plastic, but still only transmits at most about 40% of the light.

5. **Laboratory Basic Science proposal.** If the experiments this summer and the proposed ride-along experiment have positive results, we would like to write a LBS proposal for engineering design and construction of a getter-type detector system to be tested on OMEGA.

This material is based upon work supported by the Department of Energy [National Nuclear Security Administration] University of Rochester "National Inertial Confinement Program" under Award Number(s) DE-NA0004144.

[1] M. Kanga, Y. Hub, H. Hua and S. Zhub, Journal of Cosmology and Astroparticle Physics **2012**, 011 (2012).
[2] J. Melendez and I. Ramirez, Astrophys. J. **615**, L33 (2004).
[3] M. Asplund et al., Astrophys. J. **644**, 229 (2006).
[4] V.G. Kiptily, F. E. Cecil, and S. S. Medley. Plasma Physics and Controlled Fusion **48**, R59 (2006).
[5] S.S. Medley and H. Hendel, Princeton Plasma Physics Laboratory Report #1950 (1980).
[6] F.E. Cecil and D.E. Newman, Nucl. Instrum. Methods. **221**, 449 (1984).
[7] Y. Kim et. al., Phys. Rev. **C85**, 061601 (2012).
[8] D.A. Boyd, D.J. Campbell, J.G. Cordey, W.G.F. Core, J.P. Christiansen, G.A. Cottrell, L.G. Eriksson, T. Hellsten, J.J. Jacquinot, O.N. Jarvis, P.R. Thomas, P. v. Belle, and J.A. Wesson, Nuclear Fusion **29,** 593 (1989).
[9] F.E. Cecil and S.S. Medley, Nucl. Instrum. Methods **271,** 628 (1989).
[10] T. Nishitani, K. Tobita, Y. Kusama, and Y. Shibata, Rev. Sci. Instrum. **72**, 887 **(**2001).

[11] S.N. Abramovich, B.Ya. Guzhovskij, V.A. Zherebtsov, and A.G. Zvenigorodskij, International Nuclear Data Committee Report INDC(CCP)-326/L+F, (1991).
[12] A.J. Koning, S. Hilaire and M.C. Duijvestijn, “TALYS-1.0”, Proceedings of the International Conference on Nuclear Data for Science and Technology, April 22-27, 2007, Nice, France, editors. O.Bersillon, F.Gunsing, E.Bauge, R.Jacqmin, and S.Leray, EDP Sciences, 2008, p. 211-214.
[13] Katelyn Cook, “Measurement of Low-Energy Nuclear Cross Sections Using Inertial Confinement Fusion,” B.S. thesis, Houghton College, 2019.
[14] Tyler Kowalewski, “Inertial Confinement Fusion as a Tool to Study Fundamental Nuclear Science,” B.S. thesis, Houghton College, 2021.
[15] Micah Christensen, “An Experiment to Simulate the Trapping and Detection of Radioactive Isotopes Produced In ICF Implosions,” B.S. thesis, Houghton College, 2022.
[16] Mark Yuly, Stephen Padalino, Micah Coates and Katelyn Cook, “A possible measurement of the 3H(t,γ)6He cross section at low energy,” in Nuclear and Plasma Diagnostics for the EP-OMEGA and MTW Laser Systems, LLE Proposal for Subaward 416231-G, 2016 (unpublished).
[17] Mark Yuly, Stephen Padalino, Micah Coates and Katelyn Cook, “A Phoswich Detector System to Measure the 3H(t,γ)6He Cross Section using ICF” in Nuclear and Plasma Diagnostics for the EP-OMEGA and MTW Laser Systems, LLE Proposal for Subaward 416231-G, 2017 (unpublished).
[18] Mark Yuly, Stephen Padalino, Emma Bruce, Katelyn Cook, and Sarah Hull, “Measuring Low Energy Nuclear Cross Sections using ICF,” in Nuclear and Plasma Diagnostics for the EP-OMEGA and MTW Laser Systems, LLE Proposal for Subaward 416231-G, 2018 (unpublished).
[19] Mark Yuly, Stephen Padalino, Tyler Kowalewski, Salvatore Ferri and Steven Raymond, “Inertial Confinement Fusion as a Tool to Study Fundamental Nuclear Science,” in Nuclear and Plasma Diagnostics for the EP-OMEGA and MTW Laser Systems, LLE Proposal for Subaward 416231-G, 2019 (unpublished).
[20] Mark Yuly, Stephen Padalino, Micah Christensen, Joshua Bowman, “Progress toward using ICF to measure light-ion nuclear cross sections” in Nuclear and Plasma Diagnostics for the EP-OMEGA and MTW Laser Systems, LLE Proposal for Subaward 416231-G, 2020 (unpublished).
[21] S.Agostinelli et al., NIM **A506**, 250 (2003); J. Allison et al., IEEE Trans. Nuc. Sci. **53**, 270 (2006); J. Allison et al., NIM **A835** 186 (2016).
[22] Mark Yuly, Stephen Padalino, Adam Brown, Micah Christensen, Micah Condie, “Trapping and detecting trace radioactive isotopes produced in ICF implosions,” in Nuclear and Plasma Diagnostics for the EP-OMEGA and MTW Laser Systems, LLE Proposal for Subaward 416231-G, 2021 (unpublished).
[23] James McLean, Vizma Leimanis, Pranish Shrethsa, and Jessica Dawson, “Exploding Radioactive Wire Project” in Nuclear and Plasma Diagnostics for the EP-OMEGA and MTW Laser Systems, LLE Proposal for Subaward 416231-G, 2021 (unpublished).
[24] Rene Brun and Fons Rademakers, Nucl. Inst. & Meth. In Phys. Res. A **389**, 81-86 (1997).
[25] F. James, CERN Report No. CERN-D-506, 1994 (unpublished).
[26] https://www.caen.it/subfamilies/730-digitizer-family/
[27] https://www.digital-loggers.com/api.html
[28] https://www.raspberrypi.com/documentation/computers/raspberry-pi.html